

S.L. Sheehe and S.I. Jackson, "Spatial Distribution of Spectrally Emitting Species in a Nitromethane-Air Diffusion Flame and Comparison with Kinetic Models", In press with Combustion and Flame, October 2019.

Spatial Distribution of Spectrally Emitting Species in a Nitromethane-Air Diffusion Flame and Comparison with Kinetic Models

Suzanne L. Sheehe and Scott I. Jackson

Shock and Detonation Physics Group

Los Alamos National Laboratory, NM 87545, USA

Abstract

Current nitromethane kinetic schemes do not fully capture the intermediate reaction states of deflagrating nitromethane, which is an explosive used in many combustion applications. There is a need for data on these transient species that can be used to validate and improve contemporary kinetic models. This work aims to analyze the evolution of identified transient species present in a nitromethane-air flame stabilized on a wick at ambient pressure. We detect several new emitters in excited electronic states, $\text{HNO}^*(A')$, $\text{CN}^*(A^2\Sigma)$, NO_2^* , and in ground electronic states, CH, OH, NH, and H_2O . We also confirm the presence of previously observed reaction species $\text{CH}^*(A^2\Delta)$. Formaldehyde and the characteristic $\text{C}_2^*(A^3\Pi_g)$ swan bands are not observed. Results are reported as a function of flame position. Flame simulations for the nitromethane flame using reaction mechanisms by Brequigny et al. (*Proc. Combust. Inst.* 2014, 35, 703) and Mathieu et al. (*Fuel* 2016, 182, 597) yield good qualitative agreement to the experimental data for rich stoichiometries. While current mechanisms do not include excited state species, these results also provide insight into potential ground state precursors.

Keywords

S.L. Sheehe and S.I. Jackson, "Spatial Distribution of Spectrally Emitting Species in a Nitromethane-Air Diffusion Flame and Comparison with Kinetic Models", In press with Combustion and Flame, October 2019.

Nitromethane, diffusion flame, emission spectroscopy, flame structure, kinetic modeling

1. Introduction

Nitromethane has long been of interest as a fuel due to its high lubricity and ability to reduce engine octane numbers. It is the simplest fuel containing a nitro functional group, making it appealing for investigations of reactions involving the mutual sensitized oxidation of hydrocarbons and nitrogen oxides [1-10]. As nitromethane is also able to decompose as a monopropellant, it can also serve as a prototype for more complex energetic materials. For example, current understanding of RDX (cyclotrimethylenetrinitramine, $C_3H_6N_6O_6$) combustion is heavily reliant on nitromethane studies [1].

Due to this interest, a number of kinetic mechanisms for nitromethane decomposition and combustion with oxygen have recently been proposed [1, 2, 4, 7]. Tian et al (2009) [1] and Zhang et al (2013) [2] developed a reaction mechanism using experimental flame structure results from premixed nitromethane-oxygen flames at low pressures (approx. 76 torr). Brequigny et al (2015) [4] adapted this mechanism to higher pressures using flame speed measurements to include 702 reactions and 90 species. Mathieu et al (2016) [7] also proposed a mechanism with 1204 reactions and 172 species which incorporates elements of prior work [4, 11-19], the nitromethane sub-mechanism from Brequigny et al [4], and new decomposition data from shock tubes [20]. The two reaction mechanisms are extensively compared in [9]. The study found that the Brequigny reaction mechanism tends to be more reactive as it predicts shorter ignition delay times. It is also very sensitive to reactions involving HNO while the Mathieu mechanism is sensitive to those involving conversion between NO and NO₂. A

S.L. Sheehe and S.I. Jackson, "Spatial Distribution of Spectrally Emitting Species in a Nitromethane-Air Diffusion Flame and Comparison with Kinetic Models", In press with Combustion and Flame, October 2019.

sensitivity analysis in [9] demonstrates that both reaction mechanisms are highly sensitive to the same four reactions even though they both handle these reactions a little bit differently. Validation studies comparing predictions using these two most recent mechanisms (Brequigny et al 2015 [4] and Mathieu et al 2016 [7]) with experimental data have found deviations with shock tube ignition, flame structure, laminar burning velocity, and flame height measurements [5-10]. Such deviations suggest the need for improved nitromethane kinetic mechanisms derived from experimental observation. The individual species in the kinetic have largely not been measured experimentally in flames for pressures above 10 torr, with the exception of the recent work in [8,9]. This work looks to identify species present in nitromethane flames and present a diagnostic platform that can provide a path forward for further mechanism development.

Nitromethane chemistry has been observed to occur in distinct zones or steps [21-29]. For example, modeling has predicted a wide reaction zone exists for liquid nitromethane flames that can be divided into three zones [27]: (i) consumption of nitromethane yielding peak concentrations of NO, CH₄, CH₂O, HONO, and HNO, (ii) peak concentration of N₂O and consumption of CH₂O, N₂O, and HNO, and (iii) total consumption of NO and CH₄. The underlying chemistry associated with initiation remains an open question. For instance, in [27], the initiation step in the combustion is C-N bond fission, yielding CH₃ and NO₂, with subsequent branching reactions. There is still debate if there is a parallel initiation step where CH₃NO₂ undergoes rearrangement via a roaming pathway to methyl nitrite CH₃ONO* with subsequent unimolecular decomposition to CH₃O and NO [7, 9, 20, 30-32]. The initiation reaction in

S.L. Sheehe and S.I. Jackson, "Spatial Distribution of Spectrally Emitting Species in a Nitromethane-Air Diffusion Flame and Comparison with Kinetic Models", In press with Combustion and Flame, October 2019.

Brequigny [4] is the single step fission of the C-N bond, while the Mathieu mechanism includes both parallel initiation pathways. Mathieu et al [7] emphasizes that the reaction rate utilized for the parallel initiation pathway is taken from theory. In order to answer questions regarding nitromethane chemistry, including the initiation pathways, direct observation of species is needed. It is the goal of this work to further resolve the reaction zone structure through identification of species in a nitromethane flame.

Prior works have identified a need for (1) increased characterization of the chemical flame structure in nitromethane-air deflagration and (2) improved understanding of the excited state species on the reaction kinetics (as existing mechanisms generally only include ground state species). Emission spectroscopy measurements are able to address both needs by identifying species present at various flame locations from analysis of their spectral emissions. These emitters are highly dependent on local ground state species and can therefore be used to identify local ground state species and associated pathways. For example, Grebe and Homann (1982) [33] demonstrated that the concentrations of the emitters in a flame could be quantitatively simulated and correlated to simultaneous formation of hydrocarbons (and key intermediates) in the system of study. More recently, emitters in flames have been used as intrinsic indicators for the state of combustion to infer basic properties such as local stoichiometry and heat release [34-41]. Therefore, emission spectra can be used as another tool to assist in the characterization of the combustion chemistry.

Emission spectroscopy has been applied successfully to nitromethane flames in the ultra violet-visible (UV-VIS) region (200-450 nm) [21, 24-25]. In these studies, two distinct regions

S.L. Sheehe and S.I. Jackson, "Spatial Distribution of Spectrally Emitting Species in a Nitromethane-Air Diffusion Flame and Comparison with Kinetic Models", In press with Combustion and Flame, October 2019.

were observed: (i) an inner flame core attributed to self-sustained combustion, and (ii) an outer flame shell thought to be air-supported combustion. In lower pressure environments, approx. 10 kPa, nitromethane-air and nitromethane-oxygen flames exhibit an orange broadband continuous broadband emission in the inner zone and the following emitters in the outer zone: $C_2^*(A^3\Pi_g)$, $CH^*(A^2\Delta)$, $CN^*(B^2\Sigma)$, $OH^*(A^2\Sigma^+)$, $NH^*(A^3\Pi)$, and $NO^*(A^2\Sigma)$ [20]. In atmospheric and higher pressure environments, the same set species were also detected in nitromethane pool fire flames, except for $C_2^*(A^3\Pi_g)$ and $CH^*(A^2\Delta)$ [23-24]. Formaldehyde emission was not observed in any of these flames, although it has been seen in shock tube studies [42-43].

In this work, we address the lack of detailed nitromethane flame emission measurements in the visible and near-infrared (VIS-NIR) region (400 – 975 nm). A low-resolution broad-spectrum spectrometer was utilized, resulting in the single shot capture of a broad number of emitting species. The laminar diffusion flame was stabilized on a cylindrical aluminum oxide wick. Time-averaged measurements at a well-defined spatial resolution and emission spectra were taken as a function of flame height and radial position. These data were used to evaluate two different contemporary reaction mechanisms based on their ability to both predict the presence of the observed species and to accurately predict the order in which emitting species appear in the flame.

2. Experimental Method

A laminar diffusion flame is stabilized on a candle, which consists of a brass annulus, wick, and test-tube, as depicted in Fig. 1. The brass annulus holds the wick securely via a set-screw. The quartz test-tube with a volume of 35 mL contained a reservoir of liquid fuel that

S.L. Sheehe and S.I. Jackson, "Spatial Distribution of Spectrally Emitting Species in a Nitromethane-Air Diffusion Flame and Comparison with Kinetic Models", In press with Combustion and Flame, October 2019.

was varied between experiments to hold either: (i) nitromethane, (Acros Organic, 99+% for analysis), (ii) perdeutero-nitromethane, (CD_3NO_2 , Aldrich, 99% atom D), or (iii) methanol (CH_3OH , Fisher Chemical, Acetone free, Absolute). The cylindrical aluminum oxide fibrous wick was machined with diameter $6.0 \text{ mm} \pm 0.5 \text{ mm}$ from a type Buster-M35 ceramic insulation board (Zircar Zirconia, New York). The board is a capillary network of pressed micro-fibers which draws the fuel up to the wick surface via surface tension.

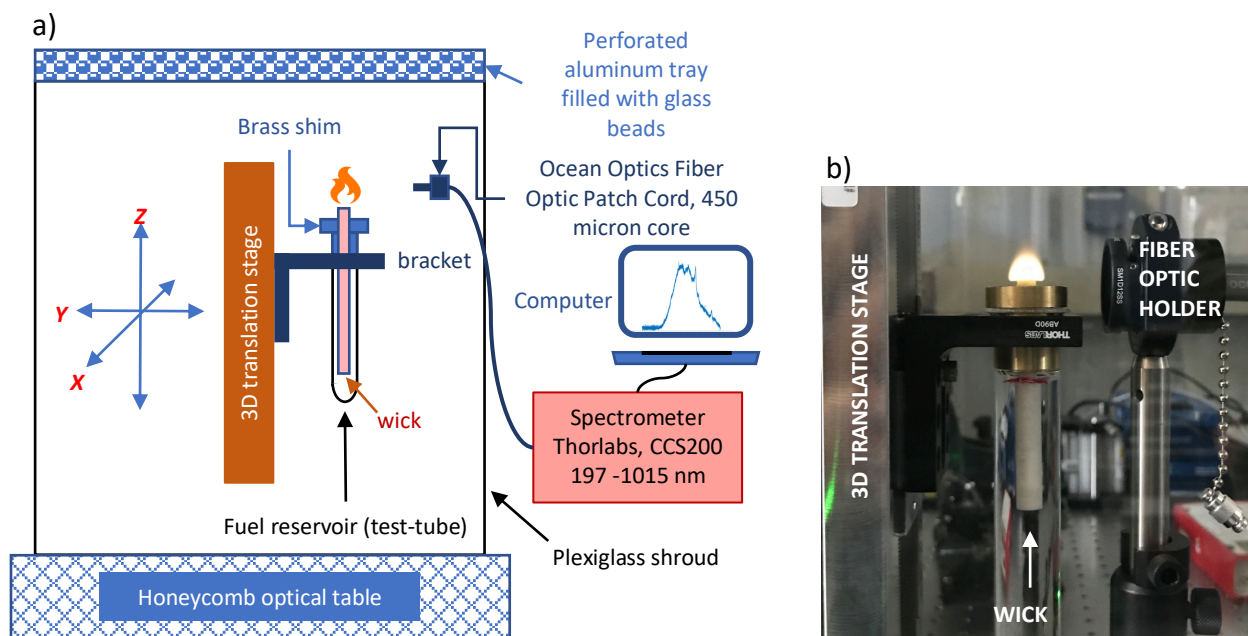


Fig. 1. Schematic of experiment: a) cartoon drawing and b) framing camera

The candle was bracket mounted to a three-axis translation stage (Velmex Inc. New York) with a resolution of 0.25 mm. To ensure a steady flame, the candle and translation stage assembly was housed in a clear pexiglass shroud. Damped airflow is facilitated via a porous metal base and a perforated aluminum tray top filled with glass beads. Thus, the flame was at ambient pressure, which was measured to be 0.766 atm (77.6 kPa) at Los Alamos National Laboratory.

S.L. Sheehe and S.I. Jackson, "Spatial Distribution of Spectrally Emitting Species in a Nitromethane-Air Diffusion Flame and Comparison with Kinetic Models", In press with Combustion and Flame, October 2019.

With this procedure and setup, the resulting flame was steady, laminar, and repeatable over the course of five minutes. The flame was low-sooting, but it only takes a few small soot particles in a wick capillary to introduce flow instabilities. Such instabilities became noticeable after the duration of five minutes. The collection of multiple averaged spectrum exceeds five minutes and formation of instabilities increases with increasing time, so the wick was cleaned after three minutes, which is the duration of a single averaged spectrum.

Flame emission was collected using a 1-m-long Ocean Optics solarization resistant SMA patch cord optical fiber that was transparent from 200-1100 nm with a core of $450 \pm 8 \mu\text{m}$ and numerical aperture of 0.2. The fiber end was set at $11.9 \pm 0.5 \text{ mm}$ from the origin (i.e. center of the wick surface). The fiber was directly connected to a low-resolution Czerny-Turner spectrometer with a $20 \mu\text{m}$ by 1.2 mm slit (Thorlabs CCS200) that disperses light onto a CCD 3648-pixel line array using a 600 lpmm grating. This yielded a FWHM spectral resolution of approximately 1.5 nm. The experimental data presented in this work is comprised of many individual averaged integrations, each obtained at a single location. Emission was measured at eight different flame heights and seven different radial locations. The integration time for a single measurement ranged from 4-15 seconds, depending on the flame emission level and averaged multiple measurements over the course of three minutes. The total integration time for all measurements was approximately 207 minutes. Spectra were corrected for dark current and system response (wavelength-intensity). Multiple repetitions of the experiment performed on different days showed a difference of approximately 6%. Spectral identification of emitting species in the nitromethane flame using the three different fuels (nitromethane, perdeutero-

S.L. Sheehe and S.I. Jackson, "Spatial Distribution of Spectrally Emitting Species in a Nitromethane-Air Diffusion Flame and Comparison with Kinetic Models", In press with Combustion and Flame, October 2019.

nitromethane, and methanol) is presented and discussed in [44]. Some results from the perdeutero-nitromethane flame is further discussed in the subsequent text.

Wavelength response was calibrated to atomic emission from fiber coupled neon, argon, and zinc lamps (Avantes, AvaLight-CAL-Neon-Mini, AvaLight-CAL-Argon-Mini, AvaLight-CAL-Zinc), and verified against flame emission of Na and CaOH that was generated by sprinkling NaCl and CaCl₂ (Aldrich, 99.99%) salts onto the wick prior to ignition. Wavelength positions of the Na* emission bands were found to within ± 0.4 nm of those found in the literature [44], thus indicating an uncertainty of ± 0.4 nm along the wavelength axis.

After wavelength corrections, intensity calibrations were performed using two NIST-traceable lamps, a 200-W-quartz-halogen-tungsten-filament lamp with output 3280 K (Oriel Part# 63355) and a deuterium lamp (Ocean Optics, DH-3plus). In both cases dark and light spectra were averaged over six minutes. A 10% discrepancy was found between the two lamp calibrations; therefore, the uncertainty is estimated to be approximately 10%. These quantitative emission intensities were utilized in this work to qualitatively describe molecular concentration because emission intensity is linearly proportional to number density. No attempt has been made to quantitatively calculate molecular concentrations. These limits are described further in Appendix A.

Figure 2 shows typical images of the nitromethane flame taken in the visible spectrum. The flame measures approximately 11 mm in diameter and 6-8 mm in height. As can be seen in the right image, (b), the flame appears transparent throughout the flame sheet. In the left image, (a), the metal ruler partially reflects the flame emission and enables visualization of the

S.L. Sheehe and S.I. Jackson, "Spatial Distribution of Spectrally Emitting Species in a Nitromethane-Air Diffusion Flame and Comparison with Kinetic Models", In press with Combustion and Flame, October 2019.

flame boundaries. Here, the flame appears white, lifted, and to slightly wrap around the wick.

The flame is semi-transparent, visibly steady, and laminar.

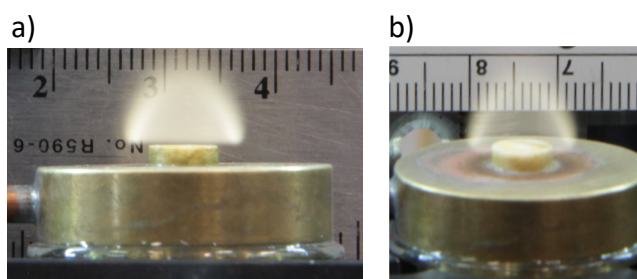


Fig. 2. Two perspectives of the nitromethane-air diffusion flame stabilized on the wick: a) metal ruler in background and b) white ruler in background

3.0. Results

3.1. Centerline spectra and detected species

Figure 3 shows centerline spectra of the nitromethane diffusion flame from six flame heights (z-axis) above the wick surface with spectral assignments for the most intense bands. The emission spectra show characteristic bands for $\text{CH}^*(A^2\Delta)$, $\text{HNO}^*(A^1A'')$, $\text{CN}^*(A^2\Pi)$, NO_2^* , CH, OH, NH, H_2O , and Na^* (a contaminant). The assignments include electronic transitions (denoted with *) and ground state vibrational-rotational transitions. Consistencies with prior nitromethane flame measurements are observable. First, transitions from the $\text{CH}^*(A^2\Delta)$ electronic state and a different CN^* state, ($B^2\Pi$), have been previously observed in low pressure (approx. 10.67 kPa) and atmospheric flames [21, 24-25]. Additionally, NO_2^* emission was also present in prior emission spectra, but not explicitly noted [21, 24-25].

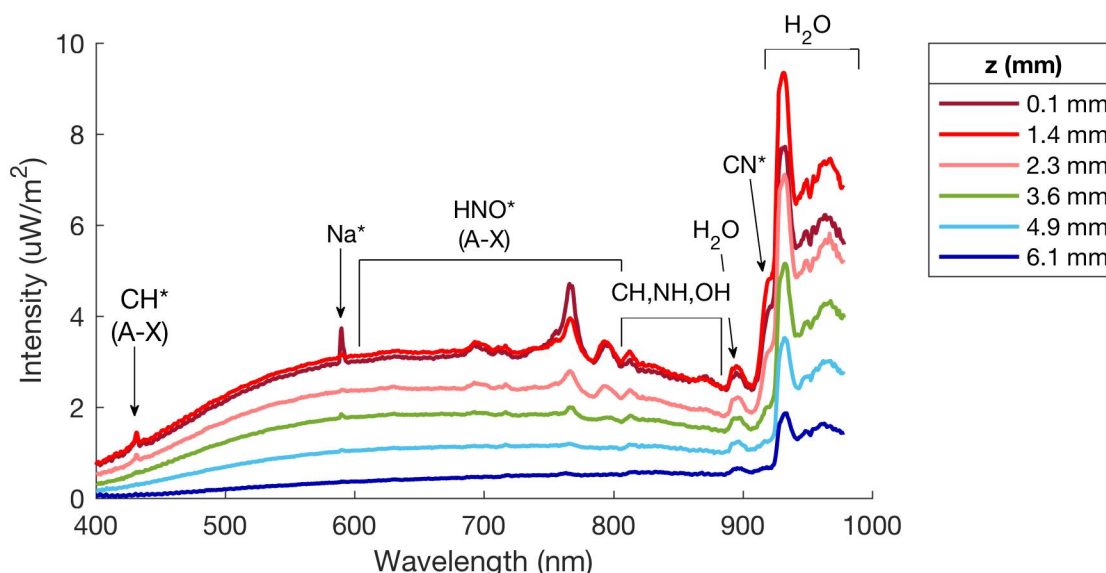


Fig. 3. Corrected emission spectra taken at various flame heights (z) along the centerline of the nitromethane diffusion flame with spectral assignments.

There are also several measurements novel to this work. While ground state HNO has previously been detected using a combination of tunable vacuum ultraviolet photoionization and mass spectrometry [1], this is the first measurement of HNO* emission in nitromethane flames. Furthermore, this work characterizes the transitions of CH, OH, NH, and H₂O, which have not been previously observed in nitromethane flames. Here, the measurements in the VIS-NIR region allow for such analysis.

3.2. Verification of flame transparency

Measurements were taken at different radii (x) to illustrate the transparency of the flame core. The emission spectra collected in this work are integrated line-of-sight measurements where the fiber optic collects all emitted photons within its cone of acceptance. As seen in Fig. 2, the images show that the nitromethane flame is relatively transparent and

that the flame core is thus visible to the fiber probe. Measurements at varying radii (x) confirm this assessment.

The variation across the flame width demonstrates that the measurement penetrates the flame core due to the variation in intensity across the flame width. That is, a transparent flame would have a varying flame thickness, with highest amplitude across the thickest part of the flame, which correlates with the observations of this work. Note that these trends are approximate due to beam steering which results from geometry, temperature, and composition. These effects are largely neglected because this work is focusing on qualitative trends. Figure 4 shows the emission intensity of the H₂O (003-000) vibrational transition near 895 nm versus z position for five radial locations. (Note that emission intensity is integrated over the entire band envelope, as described in Appendix A.) Above the wick surface ($z > 0$), the maximum is along the centerline and consistent with a transparent flame core. Below the wick surface ($z < 0$), the maximum is off-center because the line-of-sight along the centerline is obstructed by the wick. Optically thick flames would have a flat profile across the flame width.

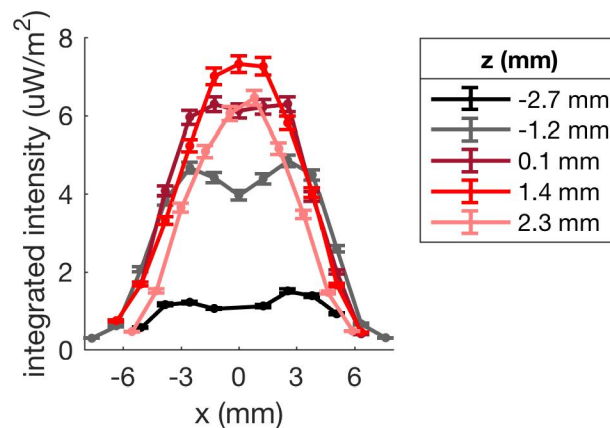


Fig. 4. Emission intensity of water band centered near 895 nm as a function of x for five different z . Error bars represent the approx. 6% variation in data from multiple experimental repetitions.

Weak water emission is also apparent below the wick surface due to flame wrapping around the wick edge (also seen in Fig. 2). Below the wick surface, the emission has a dip about the centerline that coincides where the wick shortens the measurement pathlength. This depression disappears above the wick surface where the pathlength is no longer physically shortened by the wick. Separate measurements performed with perdeutero-nitromethane exhibit no water emission in the region of 895, or 920-980 nm indicating that the detected emission was not due to thermally excited ambient water [44]. Thus, the observed water emission is a combustion product.

3.3. Emission profile variation with radius

The variation of the emission intensity versus height is shown for different radial locations in Fig. 5 for all eight identified emitters (CH^* , HNO^* , NO_2^* , CN^* , H_2O , CH , NH , and OH). The emission intensities were integrated in similar fashion to the H_2O profiles of Fig. 4 with integration details for each molecule in Appendix A. Several trends are observed. First, each profile exhibits a maximum. For several species (including CN^* , H_2O , NH , CH , and OH), the maximum height decreases with increasing radius. Some species profiles exhibit more than one local maximum, notably NH and OH . Also, the intensity of the profile generally decreases with increasing radius. All species show emission below the wick surface resulting from flame wrapping, consistent with the prior observation for water. These observations are consistent with the visual shape of the flame.

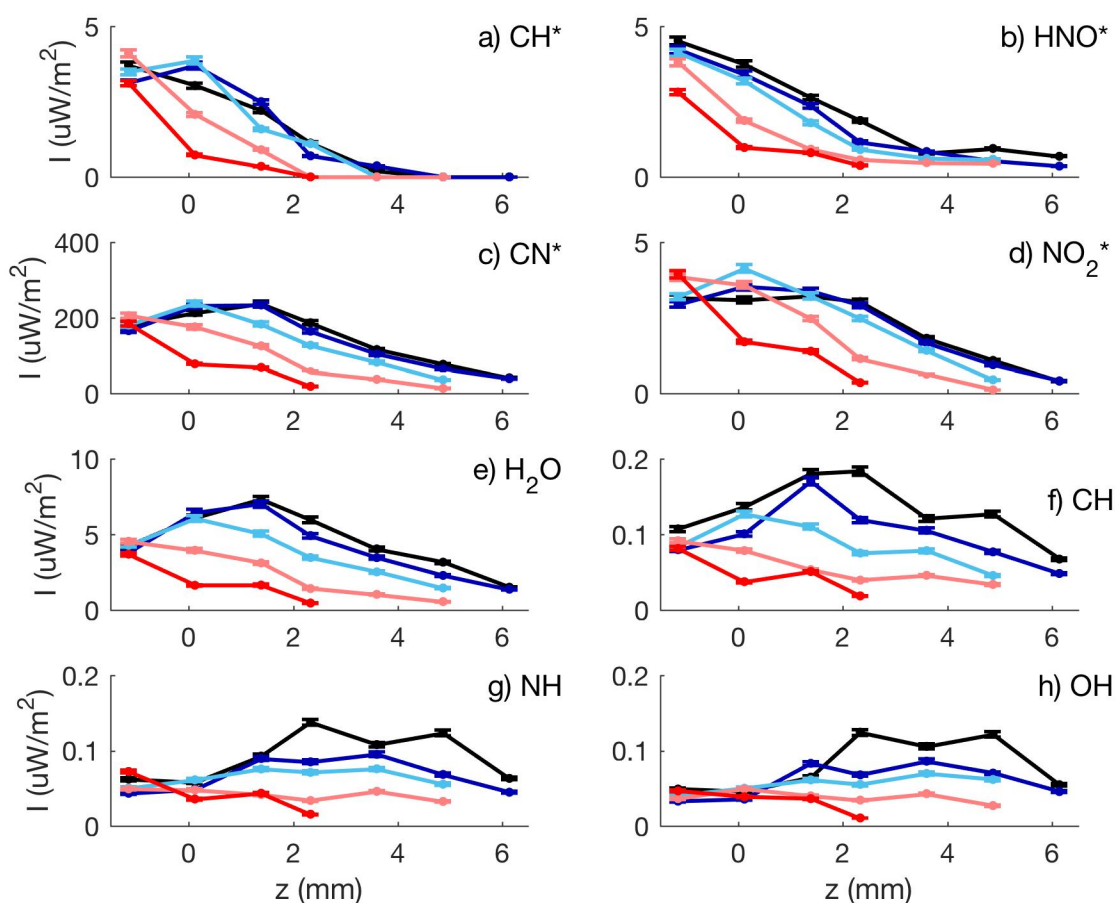


Fig. 5. Reported emission intensity, I , versus z for five different x : 0 (black), -1.3 (blue), -2.5 (light blue), -3.8 (pink), and -5.1 mm (red). Error bars represent the approx. 6% variation in data from multiple experimental repetitions.

Figure 5 shows that there is radial variation in which the order of species appear. For example, NH and OH peak at higher flame heights than CH^* and HNO^* . Table 1 summarizes the order in which the species maximum and local maxima appear for different x -positions.

Table 1: Experimental Species local maxima order along the z-axis for five different x-locations (red=maximum, blue=local maxima); Species separated by commas appear at similar heights, within the measurement resolution.

0 mm	-1.3 mm	-2.5 mm	-3.8 mm	-5.1 mm
HNO*, CH*	HNO*, NH, OH	HNO*, CH*	HNO*, NO ₂ *, CH*, CN*, H ₂ O	HNO*, NO ₂ *, CH, NH, OH, CH*, CN*, H ₂ O
NO ₂ *, CN*, H ₂ O	CH*, NO ₂ *, CN*, H ₂ O	NO ₂ *, CN*, H ₂ O, HNO*, CH, OH	CH, NH, OH, CN*, H ₂ O	CH, NH, OH,
CH, NH, OH	CH, NH, OH	CH, NH, OH	CH*	
HNO*, CH, NH, OH, H ₂ O	HNO* NH, OH	HNO*, OH	HNO*, CH, NH, OH, CN*, H ₂ O	

4.0. Discussion

4.1. Comparison of experimental data with calculated flame profiles

During operation of the flame, the liquid nitromethane is drawn to the surface of the wick by surface tension. The nitromethane at the wick surface is then diffusively heated by adjacent exothermic reactions in the gas above the wick and evaporates. Simultaneously, fresh air is drawn in horizontally across the brass surface of the wick holder. The air then flows along the wick surface, mixing with the evaporating nitromethane and rising buoyantly as it is heated.

From these observations, one expects that the nitromethane-air mixture at the center of the flame core to be of higher equivalence ratio than near the flame edge. Furthermore, the experimental measurements found that the order of peak species emission varied with radial location in the flame. Flame calculations can be used to verify if the approximate trend of these variations is consistent with radial variations in the fuel-air equivalence ratio.

S.L. Sheehe and S.I. Jackson, "Spatial Distribution of Spectrally Emitting Species in a Nitromethane-Air Diffusion Flame and Comparison with Kinetic Models", In press with Combustion and Flame, October 2019.

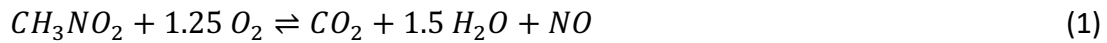
Our calculations assume that the fluid flow in the flame reaction zone is one-dimensional in the z direction to leading order, with stoichiometry varying only with radius. This assumption approximates the candle flame to be both one-dimensional and premixed by neglecting the horizontal transport induced by the wick geometry, which are traditionally important in a conventional diffusion flame. However, experimental observations indicate that the candle geometry does not operate purely as a classical diffusion flame.

During experiments, it is observed that the wick surface does not remain flooded once the flame is established. Additionally, air is present in the test tube that feeds the wick and can be also entrained into the wick with the nitromethane. Thus, it is expected that the experimental configuration will exhibit characteristics of both a premixed flame and a partially mixed diffusion flame: The outer radii will operate more as a diffusion flame, but the flame near the wick centerline is expected to behave more as a premixed flame due to little entrainment beyond the initial flame edge. Thus, while not expected to be fully accurate, the dominant chemical physics (including the order of species appearance in the flame) are expected to be captured in a 1D premixed flame calculation. As discussed below, calculations for mixtures of identical equivalence ratio in both the 1D premixed and counterflow diffusion flame geometry yield equivalent order of appearance of major species, supporting the logic behind this modeling approach.

The flame was simulated using the "Burner Flame" function in Cantera [46], which is intended to approximate a 1-D burner-stabilized flat flame for multiple equivalence ratios,

S.L. Sheehe and S.I. Jackson, "Spatial Distribution of Spectrally Emitting Species in a Nitromethane-Air Diffusion Flame and Comparison with Kinetic Models", In press with Combustion and Flame, October 2019.

$\phi=0.6, 0.8, 1.0, 1.5, 2.0, 2.5, 3.0,$ and 4.0 . The stoichiometric ratio was defined by reaction (1), which enabled direct comparison of results with previously published results [1, 2, 4-6,9]:



The flames were calculated using two different reaction kinetic mechanisms: Brequigny [4] and Mathieu [7]. The Brequigny mechanism includes all the requisite detailed transport and thermodynamic parameters, while the Mathieu mechanism does not. Calculations with Mathieu used the transport parameters from [47, 15, 4] and thermodynamic parameters of the Brequigny mechanism, as suggested in [9]. The diffusive mass flux was computed using a multi-component formulation with an unburned gas velocity of 0.03 m/s and with adaptive mesh refinement on a 0.06 m grid yielding grid spacing in the range 0.6-75 μm depending on the reaction mechanism and equivalence ratio. These same parameters were utilized in a separate 1D diffusion flame, the "counterflow diffusion flame" in Cantera, for comparison between the diffusion and premixed flame case.

From the calculations, the order of occurrence in local maxima for each species concentrations was determined. The present section discusses only the experimentally observed species that were also directly predicted by the reaction mechanism: CH, NH, OH, H₂O, and CH* (only Mathieu mechanism calculates CH*). Finally, consider that the calculations predicted species concentrations representative of electronic ground state populations summed over all rotational-vibrational internal states, while the experimental data captured only a limited number of these states.

S.L. Sheehe and S.I. Jackson, "Spatial Distribution of Spectrally Emitting Species in a Nitromethane-Air Diffusion Flame and Comparison with Kinetic Models", In press with Combustion and Flame, October 2019.

The calculated order of species peaks (local maxima) are shown in Table 2. As can be seen, equivalence ratios ($\phi = 0.6-1.5$) are qualitatively equivalent regarding predicted species order because the order is the same. At richer equivalence ratios ($\phi = 2.0-4.0$), the ordering is much different in comparison, mostly due to OH, NH, H₂O, and CH: species OH and NH have a single sharply defined peak at leaner ratios ($\phi \leq 1.5$) that breaks into a broad profile with multiple local maxima at richer ratios ($\phi > 1.5$) whereas CH and H₂O change order relative to each other at these richer ratios. These changes are illustrated in Table 2 using lines. It can be seen from Table 2, that there are numerous lines and the trends are complex.

The comparison between spectral emission intensity and predicted species fraction is qualitative. Emission intensities are linearly proportional to number density and to fluorescence efficiency, the latter of which is dominated by a quenching cross-section and is a function of pressure, temperature, and composition. The determination of accurate quenching cross section is critical for quantitative measurement, but qualitatively we can assume that it does not vary significantly (e.g, more than a few orders of magnitude) over the flame front. For extensively studied excited molecules such as OH* and NO*, this has been shown to be a valid assumption [48,49]. The quenching coefficients for molecules such as NO₂*, HNO*, NH, OH, CH, and H₂O are not well known (or not at all known), which makes extraction of species concentrations from the experimental spectra difficult.

Table 2: Predicted species order along the z-axis using reaction mechanisms proposed in Brequigny et al (2015) [4] and Mathieu et al (2016) [7]. Blue indicates local maxima and red indicates the maximum in the predicted species mole fraction profiles for 8 different equivalence ratios.

Equivalence ratio	0.6	0.8	1.0	1.5	2.0	2.5	3.0	4.0
Brequigny	CH NH H ₂ O OH							
Mathieu	CH CH* NH H ₂ O OH							

Figure 6 demonstrates the complexity in predicted mole fraction profiles and in a comparison with experiment. First, Fig. 6a illustrates predicted mole fraction profiles of NH, CH, OH, H₂O, and CH* for two ϕ (1.0 and 4.0) and two reaction mechanisms (Brequigny = solid, Mathieu = dashed). It can be seen that the profiles change significantly with ϕ . For example, OH switches from a single defined peak to a broad envelope at $\phi = 4.0$. Second, Fig. 6b shows the experimental data for the same species at two different x-positions (0 and -1.3 mm). Here, the profiles illustrate that the experimental species order change with x-position (as

summarized in Table 1). Finally, Figs. 6a and 6b illustrate that a visual comparison is not straightforward.

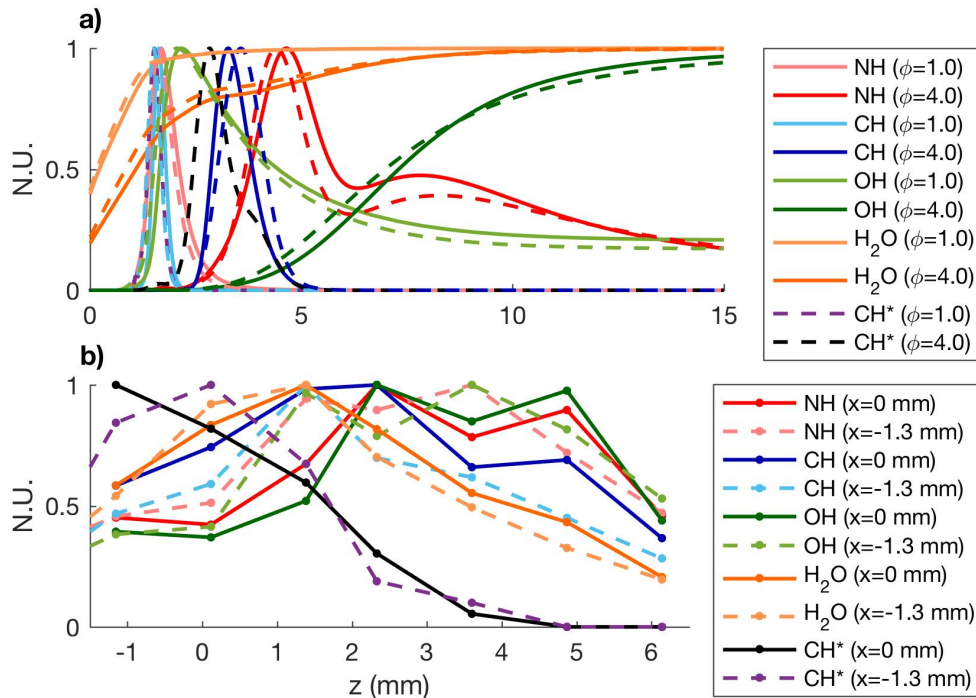


Fig. 6. Comparison of model with experiment where y-axis is normalized units (N.U.) a) Predicted mole fraction profiles, solid = Brequigny mechanism, dashed = Mathieu mechanism b) experimental profiles from $x=0$ and $x=-1.3$ mm.

Due to the complex analysis, we have developed a methodology to qualitatively compare the model and experiment that numerically ranks the agreement between experiment and each calculation using defined criteria:

1. Are the strong peaks of CH, NH, and OH in the right order relative to one another?
2. Is the maximum of H₂O in the correct place relative to the strong peaks of CH, NH, and OH?
3. Is the first OH peak (weak or strong) in the right place relative to strong peaks of CH and NH?
4. Is the second OH peak (weak or strong) in the right place relative to strong peaks of CH and NH?
5. Is the first weak OH peak in the right place relative to strong peak of CH?

S.L. Sheehe and S.I. Jackson, "Spatial Distribution of Spectrally Emitting Species in a Nitromethane-Air Diffusion Flame and Comparison with Kinetic Models", In press with Combustion and Flame, October 2019.

6. Is the second weak OH peak in the right place relative to the strong peaks of CH and NH?
7. Is the first NH peak in the right place relative to the strong NH Peak?
8. Is the CH* peak in the right position relative to the strong peaks of CH and H₂O?
(Matheiu mechanism only)

For each radial measurement plotted, higher scores indicate that the calculated equivalence ratio is more consistent with experimental data. Fig. 7 quantifies this qualitative agreement between experimental data and calculations.

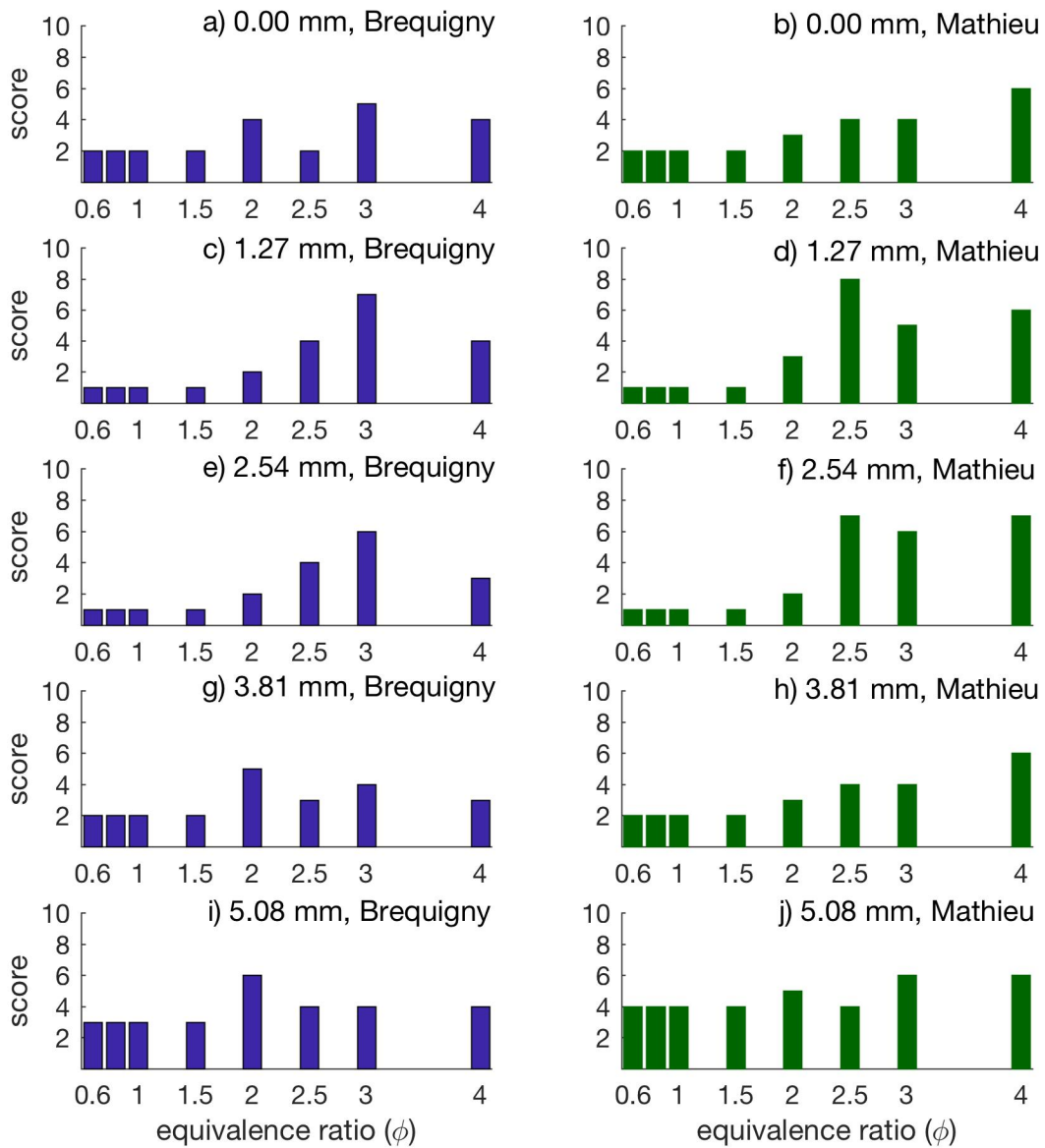


Fig. 7. Score as a function of equivalence ratio (ϕ) for each radial position (x) and reaction mechanism, Brequigny (left) and Mathieu (right).

As can be seen in Fig. 7, both mechanisms are consistent with rich flame stoichiometry within the framework of the simplified modeling approach utilized. The Brequigny calculations show good agreement with a rich diffusion flame, with ϕ decreasing from the centerline ($\phi = 3.0$) to the flame edge ($\phi = 2.0$). The Mathieu simulations are less consistent, with the best agreement

S.L. Sheehe and S.I. Jackson, "Spatial Distribution of Spectrally Emitting Species in a Nitromethane-Air Diffusion Flame and Comparison with Kinetic Models", In press with Combustion and Flame, October 2019.

at $\phi = 4.0$ for most x ($x=0.00, 2.54, 3.81, 5.08$ mm) and $\phi = 2.5$ at x between center and wick edge ($x=1.27, 2.54$). It is noted that that both the Brequigny and Mathieu mechanisms have not been calibrated for equivalence ratios greater than $\phi = 2.0$ [4,7], which could lead to discrepancies with the present experiments. Additionally, discrepancies are also possible due to the 1D calculation approximation used to model the 2D candle flame. The 1D flame structure did not appear to affect the results, as discussed above, calculations using the 1D counterflow diffusion model show that the species order for major peaks of H_2O , CH, and NH are the same as that of the rich stoichiometry in the pre-mixed flame case indicating the order of species occurrence between the rich premixed and diffusion flame is comparable.

4.2. Comparisons of predicted precursors with NO_2^* , HNO^* , and CN^* emission profiles

Measured NO_2^* , HNO^* and CN^* emission profiles cannot be compared directly with flame simulations because these species are not included in the mechanisms. However, there must exist reaction pathways for the generation of these species and several have been previously proposed [6, 32, 50]. There should be a correlation between the mole fraction profiles of reactants and experimental emission profiles. In the following subsections, suggested kinetic pathways from the literature and those currently in the mechanism are evaluated for consistency with experimental and calculated results. There is some agreement between the calculations and the experiment in which ground state species CH, NH, OH, and H_2O , giving some confidence in the kinetic mechanisms and the following qualitative analysis of potential kinetic pathways for excited state species. Note that the subsequent analysis only examines potential dominant pathways and not intended to be an exhaustive list for all

S.L. Sheehe and S.I. Jackson, "Spatial Distribution of Spectrally Emitting Species in a Nitromethane-Air Diffusion Flame and Comparison with Kinetic Models", In press with Combustion and Flame, October 2019.

pathways generating the excited state species, nor is it intended to list consumption pathways (radiative, non-radiative, reactive, etc.).

Figure 8 illustrates main reaction pathways as adapted from the presented analysis in [4, 7, 8]. Proposed reaction pathways for the generation of excited state species are highlighted in green and discussed in the subsequent sub-sections. As can be seen, fig. 8 includes the parallel initiation pathways as discussed in [7,8]. One initiation pathway is the fission of C-N bond to generate NO_2 and CH_3 . The other pathway is rearrangement to methyl nitrite with subsequent decomposition to CH_3O and NO . The products from both pathways are largely converted to CH_2O , HCO , and eventually CO . The methoxy radical does undergo reaction to form larger hydrocarbons, C_2H_x . This is of interest because these larger hydrocarbons eventually break up to form CH_2 and CH , both which have been posited to generate C_2^* [6], which could be a major component for CN^* generation (further described in sub-section 4.2.3).

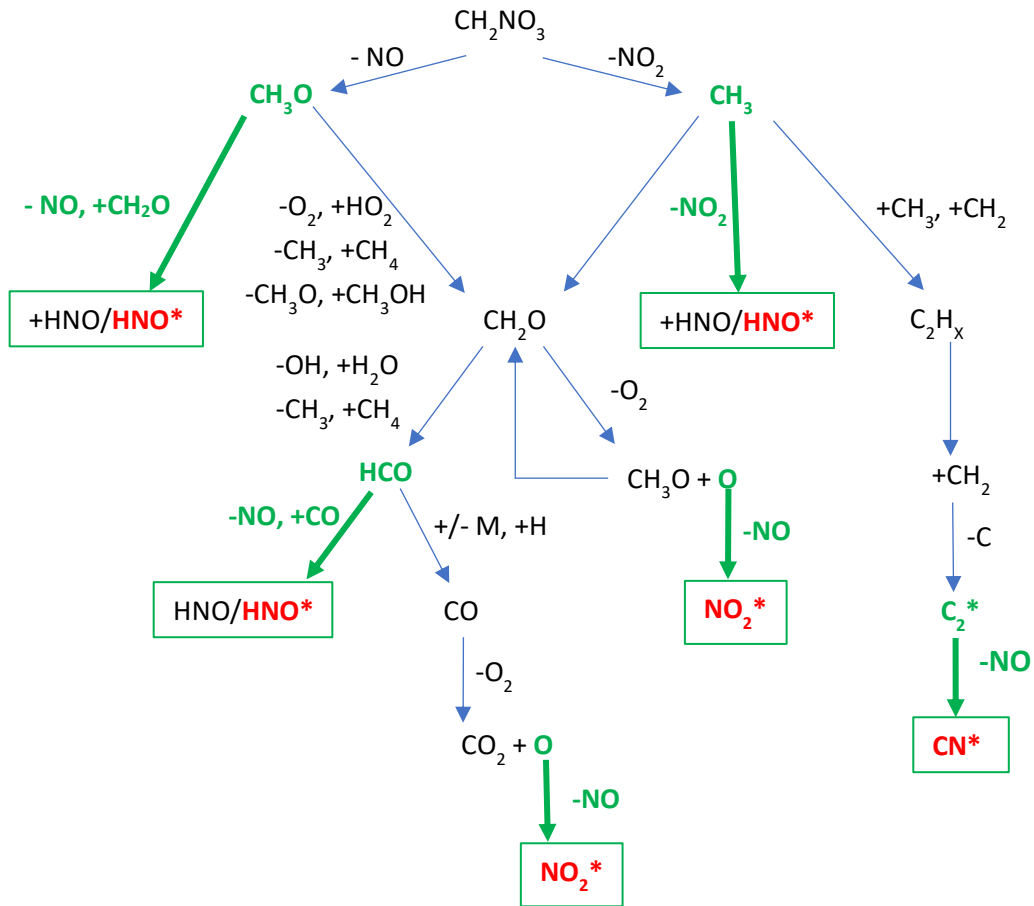


Fig. 8. Reaction pathways for the combustion of nitromethane as adapted from [4,7]. Proposed pathways for excited state pathways highlighted in green.

4.2.1 NO_2^*

NO_2^* emission has largely been demonstrated to result from the recombination of NO with atomic oxygen [51-55]. Near-simultaneous collision with a third body, 'M', is required to stabilize the NO-O collisional complex:



Prior emission spectra of NO_2^* used for comparison with experiment in [44] result from recombination of NO with atomic oxygen (Rxn. 1) and exhibit very good agreement, which

S.L. Sheehe and S.I. Jackson, "Spatial Distribution of Spectrally Emitting Species in a Nitromethane-Air Diffusion Flame and Comparison with Kinetic Models", In press with Combustion and Flame, October 2019.

indicates that observed NO_2^* emission is from Rxn. 2. However, the calculated precursor mole fractions of O and NO suggest that NO_2^* emission would peak later than observed experimentally. Based on these predictions, Rxn. 2 is unlikely to be contributing to NO_2^* emission at these early times in experimental results. While the flame geometry used in this work is weakly two-dimensional, it does have a one-dimensional streamline along with centerline by symmetry. Two-dimensional transport effects or diffusion/premixed flame effect are very unlikely to be responsible for the deviation observed here. Further work on species identification and measurement in the flame is needed to delineate additional NO_2^* pathways. In particular, measurement of O-atom concentrations in the flame would be most helpful in eliminating Rxn (2) as a dominant pathway because figure 8 does demonstrate a clear pathway to NO_2^* emission early in the flame through the oxidation of formaldehyde.

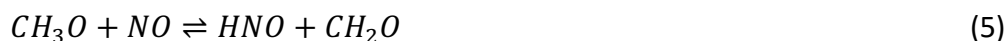
4.2.2. HNO^*

The experimental results show the occurrence of HNO^* very early in the reaction. Review of the literature indicates two reaction sets consistent with this observation [9, 19, 20, 56] and several others that are not [8,9, 55, 57-69]. The probable reaction sets assume that HNO^* is produced simultaneously with HNO, which is supported by quantum mechanical predictions that show that the HNO^* potential energy surface is relatively low lying and has conical intersections with the ground potential energy surface [64]. For example, in the reaction, $\text{OH} + \text{NH} \rightleftharpoons \text{NO} + \text{H}$, HNO^* is a transition state species [66-67]. Experiment and calculations show that HNO^* emission is not simultaneously present with NH, so this reaction pathways is not feasible for early generation of HNO^* . It should be noted that HNO^* emission

S.L. Sheehe and S.I. Jackson, "Spatial Distribution of Spectrally Emitting Species in a Nitromethane-Air Diffusion Flame and Comparison with Kinetic Models", In press with Combustion and Flame, October 2019.

was initially thought to have resulted from recombination of NO with atomic H because this is a ubiquitous result [55, 57-66], but calculations using both the premixed and the counterflow models do not indicate that HNO* results largely from recombination.

The following reactions support HNO (and thus HNO*) production early in the reaction zone [9, 20], as shown in Fig. 8:



Reaction 3 and 5 are in both mechanisms [4,7] while Rxn. 4 is not. Note that Rxns. 3 and 5 are highly dependent on the initiation pathways [9], and the two mechanisms, Brequigny and Mathieu, have different initiating pathways [4,7]. Recently, vibrationally excited (100-000) HNO was observed from Rxn. 4 [56]. This species can form directly from HNO* by emission [44]. In addition, recent experimental CH₂O profiles in Ref. [9] are also consistent with Rxn. 3 because they are seen much earlier than predicted by either the Mathieu or Brequigny mechanisms. Thus, the inclusion of Rxn. 4 in these mechanisms could yield formation and CH₂O and HNO and earlier times, which would be more consistent with prior works [9, 56] and current experimental results.

4.2.3. CN*

The formation of CN* is not well established in the literature [6], but Rxns. 6-7 have been posited as possible CN* formation paths [70-72].



S.L. Sheehe and S.I. Jackson, "Spatial Distribution of Spectrally Emitting Species in a Nitromethane-Air Diffusion Flame and Comparison with Kinetic Models", In press with Combustion and Flame, October 2019.



In Rxns. 6-7, the characteristic C_2^* swan bands are quenched. In the present work the swan bands are not observed. The lack of a C_2^* swan band in experimental spectra suggests that Rxn. 6-7 may indeed be responsible for the observed CN^* emission. If this is the case, then the presence of NO in nitromethane can be indirectly monitored by tracking CN^* emission along the reaction progress. Note that the pathway to CN^* emission in Fig. 8 shows the decomposition of larger hydrocarbons leading to CH_2 (and CH) and eventually CN^* . The intermediates CH_2 , CH, and C have been previously linked to the Swan bands resulting from C_2^* emission [6]. However, the formation of C_2^* is also not well understood and further investigation is necessitated to fully understand the connections between C_2^* , CN^* , CH, and CH_2 .

4.2.4 CH_2O^* emission

CH_2O^* emission is not observed in the present study. While CH_2O is a major intermediate in low-to high temperatures, the lack of CH_2O^* emission is consistent prior UV (200-450 nm) emission studies of nitromethane flames [21, 24-25] and with hot flames (various fuels) [45]. CH_2O^* emission is very weak, mostly owing to short radiative lifetimes originating from strong non-radiative relaxation channels, for example, singlet-triplet intersystem crossing and nonradiative relaxation to vibrationally excited levels of the ground state [73]. It is possible that CH_2O^* is formed in the present work and the nonradiative channels dominate, causing the emission to fall below the S/N limit of the optical system. As noted previously, CH_2O^* emission has been observed in shock tube studies and it maybe that nonradiative channels are less

S.L. Sheehe and S.I. Jackson, "Spatial Distribution of Spectrally Emitting Species in a Nitromethane-Air Diffusion Flame and Comparison with Kinetic Models", In press with Combustion and Flame, October 2019.

important due to lower temperatures and/or pressures. It should be emphasized that lack of CH_2O^* emission does not preclude ground state CH_2O in the nitromethane flame; it has been measured experimentally using PLIF in premixed flames [9].

5.0 Summary and Conclusions

In this study, spatially resolved emission spectra were recorded and analyzed from a nitromethane-air diffusion flame stabilized on an aluminum oxide wick. Methanol and perfluorinated nitromethane flames were studied to confirm spectral analysis and these results are presented in [44]. The nitromethane flame is visibly transparent. The following emitters were identified: $\text{CH}^*(A^2\Delta)$, $\text{HNO}^*(A^1A'')$, $\text{CN}^*(A^2\Pi)$, NO_2^* , CH, OH, NH, and H_2O [44]. Due to a lack of prior measurements in this regime, this is the first report in a nitromethane flame for all of the identified species except $\text{CH}^*(A^2\Delta)$. Emission from C_2^* and CH_2O^* was not observed. The nitromethane flame was simulated by approximating it as a 1D premixed diffusion flame in Cantera for equivalence ratios of $\phi=0.6 - 4.0$ with the mechanisms of Brequigny [4] and Mathieu [7]. Several potential reaction pathways were identified for emitting species NO_2^* , HNO^* , and CN^* .

The order of occurrence of experimental species agreed well with the calculated species order of occurrence for rich ϕ ($\phi=2.0$ and $\phi=3.0$ for Brequigny; $\phi=2.5$ and $\phi=4.0$ for Mathieu). Note that the experimental results for H_2O , CH, and OH are representative of high lying vibrational populations only while the calculated results for these same species include populations over all internal rotational-vibrational states. In addition, identified precursors (C_2^* and NO) for CN^* predictions are consistent with experimental work.

S.L. Sheehe and S.I. Jackson, "Spatial Distribution of Spectrally Emitting Species in a Nitromethane-Air Diffusion Flame and Comparison with Kinetic Models", In press with Combustion and Flame, October 2019.

HNO* and NO₂* emission is experimentally observed early in the reaction. Identified precursors for NO₂* result in predictions inconsistent with experiment while Rxns. 3-4 were identified as being probable generators for HNO*:



As such, we recommend consideration of Rxns. 3-4 for further mechanism development. In particular, current and prior experimental works [9, 56] indicate that inclusion of Rxn. 3 might yield predictions consistent with experimental results.

This work suggests a number of simplifying techniques for future measurements in a nitromethane flame, including the generation of a flat and thin flame where the equivalence ratio is controlled. The optical system could be improved by increasing: (i) spatial resolution using a lens-pinhole system, and (ii) spectral resolution using a higher dispersive grating.

Acknowledgements

We thank Dr. David Moore for helpful discussion regarding spectral assignments.

References

- [1] Z.Y. Tian, L.D. Zhang, Y.Y. Li, T. Yuan, F. Qi, An experimental and kinetic modeling study of a premixed nitromethane flame at low pressure, Proc. Combust. Inst. 32 (2009) 311-318.
- [2] K.W. Zhang, Y.Y. Li, T. Yuan, J.H. Cai, P. Glarborg, F. Qi, An experimental and kinetic modeling study of premixed nitromethane flames at low pressure, Proc. Combust. Inst. 33 (2011) 407-414.

S.L. Sheehe and S.I. Jackson, "Spatial Distribution of Spectrally Emitting Species in a Nitromethane-Air Diffusion Flame and Comparison with Kinetic Models", In press with Combustion and Flame, October 2019.

- [3] K. Zhang, L. Zhang, M. Xie, L. Ye, F. Zhang, P. Glarborg, F. Qi, An experimental and kinetic modeling study of premixed nitroethane flames at low pressure, Proc. Combust. Inst. 34 (2013) 617-624.
- [4] P. Brequigny, G. Dayma, F. Halter, C. Mounaim-Rousselle, T. Dubois, P. Dagaut, Laminar burning velocities of premixed nitromethane/air flames: an experimental and kinetic modeling study, Proc. Combust. Inst. 35 (2015) 703-710.
- [5] J.D. Nauc ler, E.J.K. Nilsson, A.A. Konnov, Laminar burning velocity of nitromethane plus air flames: a comparison of flat and spherical flames, Combust. Flame 162 (10) (2015) 3803-3809.
- [6] J.D. Nauc ler, Y. Li, E.J.K. Nilsson, H.J. Curran, A.A. Konnov, An experimental and modeling study of nitromethane + O₂ + N₂ ignition in a shock tube. Fuel 186 (2016) 629-638.
- [7] O. Mathieu, B. Giri, A.R. Agard, T.N. Adams, J.D. Mertens, E.L. Petersen, Nitromethane ignition behind reflected shock waves: experimental and numerical study, Fuel 182 (2016) 597-612.
- [8] O. Mathieu, C. Mulvihill, and E.L. Petersen, Experimental study of nitromethane oxidation: CO and H₂O time-histories behind reflected shock waves, 911, 26th ICDERS, IDERS, Boston, MA, USA, July 30th – August 4th, 2017, paper.
- [9] C. Brackmann, J.D. Nauc ler, S. El-Busaidy, A. Hosseinia, P.E. Bengtsson, A.A. Konnov, E.J.K. Nilsson, Experimental studies of nitromethane flames and evaluation of kinetic mechanisms, Combust. Flame 190 (2018) 327-336.
- [10] M. Faghih, Z. Chen, Two-stage heat release in nitromethane/air flame and its impact on laminar flame speed measurement, Combust. Flame 183 (2017) 157-165.
- [11] O. Mathieu, E.L. Petersen, Experimental and modeling study on the high-temperature oxidation of Ammonia and related NO_x chemistry, Combust. Flame 162 (2015) 554-70.
- [12] O. Mathieu, J.M. Pemelton, G. Bourque, E.L. Peterson, Shock-induced ignition of methane sensitized by NO₂ and N₂O, Combust. Flame 162 (2015) 3053-70.
- [13] O. Mathieu, A. Levacque, E.L. Petersen, Effects of N₂O addition on the ignition of H₂-O₂ mixtures: experimental and detailed kinetic modeling study, Int. J. Hydrogen Energy, 37 (2012) 15393-405.
- [14] O. Mathieu, A. Levacque, E.L. Petersen, Effects of NO₂ addition on hydrogen ignition behind reflected shock waves, Proceed. Combust. Inst. 34 (2013) 633-40.

S.L. Sheehe and S.I. Jackson, "Spatial Distribution of Spectrally Emitting Species in a Nitromethane-Air Diffusion Flame and Comparison with Kinetic Models", In press with Combustion and Flame, October 2019.

- [15] W.K. Metcalfe, S.M. Burke, S.S. Ahmed, H.J. Curran, A hierarchical and comparative kinetic modeling study of C1-C2 hydrocarbon and oxygenated fuels, *Int. J. Chem. Kinet.* 45 (2013) 638-75.
- [16] R. Mével, S. Javoy, F. Lafosse, N. Chaumeix, G. Dupré, C.E. Paillard, Hydrogen-nitrous oxide delay times: shock tube experimental study and kinetic modelling, *Proceed. Combust. Inst.* 32 (2009) 359-66.
- [17] G. Dayma, P. Dagaut, Effect of air contamination on the combustion of hydrogen—effect of NO and NO₂ addition on hydrogen ignition and oxidation kinetics, *Combust. Sci. Technol.* 178 (2006) 1999-2024.
- [18] R. Sivaramakrishnan, K. Brezinsky, G. Dayma, P. Dagaut, High pressure effects on the mutual sensitization of the oxidation of NO and CH₄-C₂H₆ blends, *Phys Chem. Chem. Phys.* 9 (2007) 4230-44.
- [19] P. Dagaut, P. Glarborg, M.U. Alzueta, The oxidation of hydrogen cyanide and related chemistry, *Prog. Energy Combust. Sci.* 34 (2008) 1-46.
- [20] C.J. Annesley, J.B. Randazzo, S.J. Klippenstein, L.B. Harding, A.W. Jasper, Y. Georgievskii, B. Ruscic, R.S. Tranter, Thermal dissociation and roaming isomerization of nitromethane: experiment and theory, *J. Phys. Chem. A.* 119 (28) (2015) 7872-7893.
- [21] A.R. Hall, H.G. Wolfhard, Multiple reaction zones in low pressure flames with ethyl and methyl nitrate, methyl nitrite and nitromethane, *Symp. (Int.) Combust.* 6 (1957) 190-199.
- [22] H.N. Presles, P. Vidal, J.C. Gois, B.A. Khasainov, B.S. Ermolaev, Influence of glass microballoons size on the detonation of nitromethane based mixtures, *Shock Waves* 4 (6) (1995) 325-329.
- [23] H.N. Presles, D. Desbordes, M. Guirard, C. Guerraud, Gaseous nitromethane and nitromethane-oxygen mixtures: a new detonation structure, *Shock Waves* 6 (2) (1996) 111-114.
- [24] W. Eckl, V. Weiser, M. Weindel, N. Eisenreich, Spectroscopic investigation of nitromethane flames, *Propellants, Explosives, Pyrotechnics* 22 (1997) 180-183.
- [25] S. Kelzenberg, N. Eisenreich, W. Eckl, V. Weiser, Modelling nitromethane combustion, *Propellants, Explosives, Pyrotechnics* 24 (1999) 189-194.

S.L. Sheehe and S.I. Jackson, "Spatial Distribution of Spectrally Emitting Species in a Nitromethane-Air Diffusion Flame and Comparison with Kinetic Models", In press with Combustion and Flame, October 2019.

- [26] M.O. Sturtzer, N. Lamoureux, C. Matignon, D. Desbordes, H.N. Presles, On the origin of the double cellular structure of the detonation in gaseous nitromethane and its mixtures with oxygen, *Shock Waves* 14 (1-2) (2005) 45-51.
- [27] E. Boyer, K.K. 2007, Modeling of nitromethane flame structure and burning behavior, *Proc. Combust. Inst.* 31 (2007) 2045-2053.
- [28] F. Joubert, D. Desbordes, H.N. Presles, Detonation cellular structure in NO₂/N₂O₄-fuel gaseous mixtures, *Combust. Flame* 152 (4) (2008) 482-495.
- [29] B. Khasainov, F. Viro, H.N. Presles, D. Desbordes, Parametric study of double cellular detonation structure, *Shock Waves* 23 (3) (2013) 213-220.
- [30] P.A. Vlasov, N.M. Kuznetsov, Y.P. Petrov, S.V. Turetskii, Nitromethane isomerization during its thermal decay, *Kinet. Catal.* 59 (1) 6-10.
- [31] A. Matsugi, H. Shiina, Thermal decomposition of nitromethane and reaction between CH₃ and NO₂, *J. Phys. Chem. A* 121 (22) (2017) 4218-4224.
- [32] T. Edwards, D.P. Weaver, D.H. Campbell, S. Husizer, Investigation of high pressure solid propellant combustion using emission spectroscopy, *J. Propulsion* 2 (3) (1986) 228 -234.
- [33] J. Grebe, K.H. Homann, Blue-green chemiluminescence in the system C₂H₂/O/H. Formation of the emitters CH(A²Δ), C₂(d³Π_g), and C₂H*, *Ber. Bunsenges. Phys. Chem.* 86 (1982) 587-597.
- [34] V.N. Nori, J. M. Seitzman, CH* chemiluminescence modeling for combustion diagnostics, *Proc. Combust. Inst.* 32 (2009) 895-903.
- [35] A. Brockhinke, J. Krüger, M. Heusing, M. Letzgus, Measurement and simulation of rotationally-resolved chemiluminescence spectra in flames, *Appl. Phys. B* 107 (2012) 539-549.
- [36] M. Köhler, A. Brockhinke, M. Braun-Unkhoff, K. Kohse-Höinghaus, Quantitative laser diagnostic and modeling Study of C₂ and CH chemistry in combustion, *J. Phys. Chem. A* 114 (2010) 4719-4734.
- [37] D. Alviso, M. Mendieta, J. Molina, J.C. Rolón, Flame imaging reconstruction method using high resolution spectra data of OH*, CH*, and C₂* radicals, *Int. J. Thermal Sciences* 121 (2017) 228-236.

S.L. Sheehe and S.I. Jackson, "Spatial Distribution of Spectrally Emitting Species in a Nitromethane-Air Diffusion Flame and Comparison with Kinetic Models", In press with Combustion and Flame, October 2019.

- [38] N. Docquier, S. Belhafaoui, F. Lacas, N. Darabiha, C. Rolón, Experimental and numerical study of chemiluminescence in methane/air high-pressure flames for active control applications, *Proc. Combust. Inst.* 28 (2000) 1765-1774.
- [39] A. Hossain, Y. Nakamura, A numerical study on the ability to predict the heat release rate using CH* chemiluminescence in non-sooting counterflow diffusion flames, *Combust. Flame* 161 (2014) 162-172.
- [40] S. Karanani, D. Dunn-Rankin, Visualizing CH* chemiluminescence in sooting flames, *Combust. Flame* 160 (2013) 2275-2278.
- [41] T. Kathrotia, M. Fikri, M. Bozkurt, M. Hartmann, U. Riedel, C. Schulz, Study of the H+M reaction forming OH*: kinetics of OH* chemiluminescence in hydrogen combustion systems, *Combust. Flame* 157 (2010) 1261-1273.
- [42] I.S. Zaslanko, S.M. Kogarko, E.B. Mozhukin, Y.P. Petrov, Thermal decomposition of nitromethane in shock waves, *Kinet. Catal.* 13 (1972) 1001-1005.
- [43] H. Dong, W. Yong-Guo, L. Hong-Bing, S. Zhu-Mei, Studies on high speed reaction spectrum of nitromethane under high temperature and high pressure. *Chin. J. High Press. Phys.* 8 (1994) 296-301.
- [44] S.L. Sheehe, S.I. Jackson, Identification of Species from Visible and Near-Infrared Spectral Emission of a Nitromethane-Air Diffusion Flame, technical report, LA-UR-19-23458, *Accepted for publication in the Journal of Molecular Spectroscopy, preprint available at <https://doi.org/10.1016/j.jms.2019.111185>.*
- [45] R.W.B. Pearse, A.G. Gaydon, The identification of molecular spectra, 4th ed., Chapman and Hall, U.K., 1974.
- [46] D.G. Goodwin, H.K. Moffat, R.L. Speth, Cantera: An object-oriented software toolkit for chemical kinetics, thermodynamics, and transport processes, <http://www.cantera.org>, 2017. Version 2.3.0, doi:10.5281/zenodo.170284.
- [47] A. Fomin, T. Zavlev, V.A. Alekseev, I. Rahinov, S. Cheskis, A.A. Konnov, Experimental and modelling study of (CH₂)-C-1 in premixed very rich methane flames, *Combust. Flame* 171 (2016) 198-210.
- [48] P.H. Paul, J.L. Durant, J.A. Gray, M.R. Furlanetto, Collisional electronic quenching of OH A²Σ (v'=0) measured at high temperature in a shock tube, *J. Chem. Phys.* 102 (1995) 8378

S.L. Sheehe and S.I. Jackson, "Spatial Distribution of Spectrally Emitting Species in a Nitromethane-Air Diffusion Flame and Comparison with Kinetic Models", In press with Combustion and Flame, October 2019.

- [49] J.W. Thoman, J.A. Gray, J.L. Durant, P.H. Paul, Collisional electronic quenching of NO $A^2\Sigma^+$ by N₂ from 300 to 4500 K, J. Chem. Phys. 97, (1992) 8156
- [50] A. Fontijn, C.B. Meyer, H.I. Schiff, Absolute quantum yield measurements of the NO-O reaction and its use as a standard for chemiluminescent reactions, J. Chem. Phys. 40 (1) (1964) 64-70.
- [51] D.E. Paulsen, W.F. Sheridan, R.E. Huffman, Thermal and recombination Emission of NO₂, J. Chem. Phys. 43 (2) (1970) 647-658.
- [52] K.H. Becker, W. Groth, D. Thran, The mechanism of the air-afterglow NO+O → NO₂ + *hν*, Chem. Phys. Lett. 15 (2) (1972) 215-220.
- [53] D. Golomb, N.W. Rosenberg, C. Aharonian, Oxygen atom determination in the upper atmosphere by chemiluminescence of nitric oxide, J. Geophysical Research 70 (5) (1965) 1155-1173.
- [54] K. Honma, O. Kajimoto, Crossed beam study of the reaction of van der Waals molecule O+(NO)₂ → NO₂* + NO, J. Chem. Phys. 86 (10) (1987) 5491-5499.
- [55] J.K. Cashion, J.C. Polyani, Infrared chemiluminescence from the gaseous reaction atomic H. plus NO: HNO in emission, J. Chem. Phys. 30 (1959) 317-318.
- [56] C.Y. Shi, F. Dong, S. Sun, H. Zhang, L. Guo, J.K. Feng, F.A. Kong, Reaction of CH₃ with NO₂, Chin. J. Chem. Phys. 20 (31) (2007) 31-36.
- [57] F.W. Dalby, The spectrum and structure of the HNO molecule, Can. J. Phys. 36 (1958) 1336-1371.
- [58] M.J.Y. Clement, D.A. Ramsay, Predissociation in the HNO molecule, Can. J. Phys. 39 (1961) 205-209.
- [59] M.A.A. Clyne, B.A. Thrush, Mechanism of chemiluminescent reactions Involving nitric oxide—the H+NO reaction, Discussion of the Faraday Society 33 (1962) 139-148.
- [60] T. Ishiwata, H. Akimoto, I. Tanaka, Chemiluminescent spectra of HNO and DNO in the reaction of O(³P)/O₂ with NO and hydrocarbons or aldehydes, Chem. Phys. Lett. 21 (2) (1973) 322-325.
- [61] T. Ishiwata, H. Akimoto, I. Tanaka, Chemiluminescence of HNO sensitized by O₂(¹Δ_g) in the reaction systems of O(³P) + C₃H₆ + NO + O₂(¹Δ_g)/O₂ and H+NO+O₂(¹Δ_g)/O₂, Chem. Phys. Lett. 27 (2) (1974) 260-263.

S.L. Sheehe and S.I. Jackson, "Spatial Distribution of Spectrally Emitting Species in a Nitromethane-Air Diffusion Flame and Comparison with Kinetic Models", In press with Combustion and Flame, October 2019.

- [62] N. Washida, H. Akimoto, M. Okuda, HNO formed in the H+NO+M reaction system, J. Phys. Chem. 82 (21) (1978) 2293-2299.
- [63] Y. Yoshimura, H. Ohyama, T. Hamada, T. Kasai, K. Kuwata, The internal energy distribution of HNO(\tilde{A}^2A'') formed in the reaction of H+NO, Chem. Phys. Lett. 106 (4) (1984) 271-275.
- [64] K. Honma, O. Kajimoto, Crossed-beam study of the reaction of the van der Waals molecule H+(NO)₂, J. Chem. Phys. 92 (1990) 1657-60.
- [65] R.S. Lewis, K.Y. Tang, E. K.C. Lee, Photoexcited chemiluminescence spectroscopy: Detection of hydrogen atoms produced from single vibronic level photolysis of formaldehyde (\tilde{A}^1A_2)^{*}, J. Chem. Phys. 65(7) (1976) 2910-2911
- [66] R. Guadagnini, G.C. Schatz, S.P. Walch, Global potential energy surfaces for the lowest ¹A', ³A', and ¹A'' states of HNO, J. Chem. Phys. 102 (2) (1995) 774- 783.
- [67] A. Li, C. Xie, D. Xie, H. Guo, State-to-state quantum dynamics of the O(³P) + NH(X³Σ⁻) reaction on the three lowest-lying electronic states of HNO/HON, J. Chem. Phys. 138 (2013) 024308 11pp.
- [68] J.D. Zhang, L.H. Kang, X.L. Cheng, Theoretical study of the reaction mechanism of CH₃NO₂ with NO₂, NO, and CO: the bimolecular reactions that cannot be ignored, J. Mol. Model. 21 (13) (2015) DOI 10.1007/s00894-014-2568-y 6 pp.
- [69] J.D. Zhang, L.L. Zhang, X.L. Cheng, Theoretical studies of some bimolecular reactions during the decomposition of CH₃NO₂: reactions between NO₂ and nine intermediates, J Mol Model. 23 (62) (2017) DOI 10.1007/s00894-017-3231-1 6 pp.
- [70] J.A. Vanderhoff, Spectral studies of propellant combustion: experimental details and emission results for M-30 propellant, Memorandum Report BRL-MR-3714 (1988), Aberdeen Proving Ground, Maryland, USA.
- [71] J.A. Vanderhoff, Species profiles in solid propellant flames using absorption and emission spectroscopy, Combust. Flame 84 (1991) 73-92
- [72] H. Reisler, M. Mangir, C. Wittig, The kinetics of free radicals generated by IR laser photolysis, I. Reactions of C₂($\alpha^3\Pi_u$) with NO, vinyl cyanide, and ethylene, J. Chem. Phys. 71 (5) (1973) 2109-2117.

S.L. Sheehe and S.I. Jackson, "Spatial Distribution of Spectrally Emitting Species in a Nitromethane-Air Diffusion Flame and Comparison with Kinetic Models", In press with Combustion and Flame, October 2019.

[73] R.S. Sheinson, F.W. Williams, Chemiluminescence Spectra from Cool and Blue Flames: Electronically Excited Formaldehyde," Combust. Flame 21 (1973) 221-230.

Appendix A

Reported Emission Intensities

This work assumes that emission intensities can qualitatively describe spatial molecular number density trends because emission intensity is linearly proportional to number density. As reported in [44] molecular populations are distributed over many states (electronic and vibrational-rotational). An accurate qualitative description for a molecule would capture the population distribution over all internal energy states of the molecule. Therefore, emission is integrated over as many of the recorded lines within a band as possible. This integrated emission is used as "reported emission intensities" in the text. This appendix describes the limits of these integrations for each identified molecule.

Using this integrated emission intensity to qualitatively describe number density spatial trends requires that the Einstein A-coefficients for the lines do not vary more than a few orders of magnitude and that line-shape functions are comparable. The latter condition is met because the spectrometer resolution dominates the line-shape function, regardless of flame temperature. The former condition is met only if a single vibrational band is considered for integration.

The integrated emission bands for different vibrational bands of a molecule show comparable qualitative trends. In order to capture the qualitative trends of all the vibrational bands, the integrated emission intensities of the bands are averaged.

B.1. CH*

The reported emission intensities for CH* results from integration over the A(0)-X(0) vibrational Q-branch after continuous emission has been subtracted.

S.L. Sheehe and S.I. Jackson, "Spatial Distribution of Spectrally Emitting Species in a Nitromethane-Air Diffusion Flame and Comparison with Kinetic Models", In press with Combustion and Flame, October 2019.

B.2. CN*

The reported emission intensities for CN* results from partial integration over the A(0)-X(1) vibrational ${}^2R_{21}$, R_2 , R_1 , and Q_1 branches after continuous emission has been subtracted. It is assumed that any contributions from water and continuous emission are negligible. At ~ 920 nm, the integration is truncated due to contributions from water emission.

B.3. HNO*

Each vibrational band of HNO* is integrated separately over its R- and Q- branches.

B.4. NO₂*

The emission profile attributed to NO₂* appears continuous and there are no defined vibrational bands. The reported emission intensity for NO₂* is the value at 640 nm, an area relatively free of structure and other molecules. This was done because integration over the entire continuous band would mean that Einstein A coefficients would vary widely.

B.5. CH, NH, and OH

It is not possible to integrate over various CH, NH, and OH vibrational-rotational bands because these bands all overlap with each other to some degree. The bands listed in table A1 are partially isolated. The intensities at these values are taken for the "reported emission intensity".

B.6. H₂O

The reported emission intensities for H₂O results from integration over the band centered ~ 895 and then values at 927.7, 943.8, 948.1, 954.8, 959.8, and 967.7 nm.

S.L. Sheehe and S.I. Jackson, "Spatial Distribution of Spectrally Emitting Species in a Nitromethane-Air Diffusion Flame and Comparison with Kinetic Models", In press with Combustion and Flame, October 2019.